Hexagonal versus perovskite phase of manganite $R\mathrm{MnO_3}$ (R=Y, Ho, Er, Tm, Yb, Lu)

J.-S. Zhou,[1] J. B. Goodenough,[1] J. M. Gallardo-Amores,[2] E. Morán,[2] M. A. Alario-Franco,[2] and R. Caudillo[1]
[1]*Texas Materials Institute, University of Texas at Austin, 1 University Station, C2201, Austin, Texas 78712, USA*
[2]*Lab. Altas Presiones UCM, Y Dep. Q. Inorgánica I, F[a] Quimicas, Universidad Complutense, Avda. Complutense s/n, 28040-Ciudad Universitaria, Madrid, Spain*
(Received 30 March 2006; published 19 July 2006)

The floating-zone method and high-pressure synthesis have been used to obtain the hexagonal and the perovskite $R\mathrm{MnO_3}$ (R=Y, Ho, Er, Tm, Yb, Lu) compounds. We have refined the crystal structure and characterized the compounds with measurements of magnetic susceptibility $\chi(T)$ and thermal conductivity $\kappa(T)$. The systematic change of $\kappa(T)$ below T_N found in all members of the hexagonal $R\mathrm{MnO_3}$ family shows that some spin-independent bond-length fluctuation plays an important role in the suppression of $\kappa(T)$ below T_N as well as in the paramagnetic phase. The responsible soft vibrational mode is identified. In contrast, the perovskite $R\mathrm{MnO_3}$ shows a phonon-like $\kappa(T)$ below room temperature, but with an anomalously large critical scattering at T_N. A phase diagram of transition temperatures versus the R^{3+}-ion radius for both hexagonal and perovskite phases is also given.

DOI: 10.1103/PhysRevB.74.014422 PACS number(s): 75.47.Lx, 66.70.+f, 75.40.−s

I. INTRODUCTION

The ionic radii of the Mn^{3+}, Fe^{3+}, and Ga^{3+} ions are all similar, but only for M=Fe are the $R\mathrm{MO_3}$ (R=rare earth or Y) families orthorhombic perovskites for all R if prepared under ambient pressure. Except for R=La, Pr, and Nd, the $R_3\mathrm{Ga_5O_{12}}$ garnet structure becomes competitive with the $R\mathrm{GaO_3}$ perovskite structure[1] because of the stronger tetrahedral-site preference of the Ga^{3+} ion, and high pressure is required to stabilize all members of the $R\mathrm{GaO_3}$ family as orthorhombic perovskites. Similarly, high-pressure synthesis is needed to stabilize all members of the $R\mathrm{MnO_3}$ family in the orthorhombic perovskite structure.[2] The $R\mathrm{MnO_3}$ compounds prepared by standard solid-state reaction at ambient pressure fall into two structural groups: those of Group I (R=La,…Dy) have the orthorhombic perovskite structure; those of Group II (R=Ho,…Lu,Y or Sc) have the hexagonal structure of Fig. 1(a). The R=Y, Ho, Er samples of Group II have been prepared as perovskites under ambient pressure by low-temperature chemical synthesis.[3] The room-temperature orthorhombic structure of the $R\mathrm{MnO_3}$ perovskites has the cooperative site distortions shown in Fig. 1(b) where l, m, and s represent long, medium, and short (Mn-O) bond lengths. The localized $3d^4$ configurations at the octahedral-site Mn^{3+} ions are apparently responsible for stabilizing the hexagonal structure where the cooperative site rotations of the $\mathrm{MnO_{6/2}}$ octahedra, which are responsible for the octahedral distortion, become too large. However, pressure converts the hexagonal structure to the more dense perovskite phase.

The $R\mathrm{MnO_3}$ hexagonal structure of Group II consists of close-packed layers of bipyramidal $\mathrm{MnO_5}$ sites sharing corners in the (001) planes. A cooperative tilting of the bipyramidal sites below T_C displaces the R^{3+} ions along the c axis to render the compounds ferrielectric.[4] Antiferromagnetic coupling between the spins of the close-packed Mn^{3+} ions of an (001) plane is frustrated, which significantly lowers the spin-ordering temperature T_N.[5]

Sharma *et al.*[6] have reported measurements of thermal conductivity $\kappa(T)$ on selected members of Group II that showed a suppression of $\kappa(T)$ in the paramagnetic phase. They have argued that strong spin-lattice interactions due to exchange-striction fluctuations suppress $\kappa(T)$ in the paramagnetic phase of this geometrically frustrated system. However, their work overlooks the more systematic change of $\kappa(T)$ that is presented here for the entire series of the Group II $R\mathrm{MnO_3}$ compounds (R=Y, Ho, Er, Tm, Yb, Lu).

We have grown high-quality single crystals of all the hexagonal compounds by float-zone melting, and we have prepared them in the perovskite phase with high pressure. The availability of the hexagonal crystals has allowed us to observe a systematic change of $\kappa(T)$ with R^{3+}-ion radius below as well as above T_N. From these data together with recent powder neutron-diffraction data for $\mathrm{YMnO_3}$ taken from the literature,[7] we are able to conclude that a spin-independent rattling motion of the Mn^{3+} ion, which is not a Jahn-Teller (JT) ion in the hexagonal phase, is the dominant factor for suppressing $\kappa(T)$. Moreover, we compare the magnetic transition of the hexagonal and perovskite phases of the $R\mathrm{MnO_3}$ Group II compounds that we obtained with $\kappa(T)$ and magnetic-susceptibility, $\chi(T)$, measurements. Although the perovskite phases of the Group II $R\mathrm{MnO_3}$ compounds were first synthesized under pressure decades ago, the structures of the entire family have not previously been refined with the full-profile method. Therefore, we also report the structural data for the perovskite phase of the Group II $R\mathrm{MnO_3}$ compounds.

II. EXPERIMENT

Single-crystal samples of $R\mathrm{MnO_3}$ (R=Y,Ho,…Lu) were grown with an infrared-heating image furnace in flowing air. A mirror-like facet appearing on one side of the ingots was identified with Laue back diffraction to be the hexagonal plane normal to the c axis. This feature also indicates that the as-grown ingots (5 mm diameter, 50 mm long) are single domain. Ceramic samples of the hexagonal phase were used

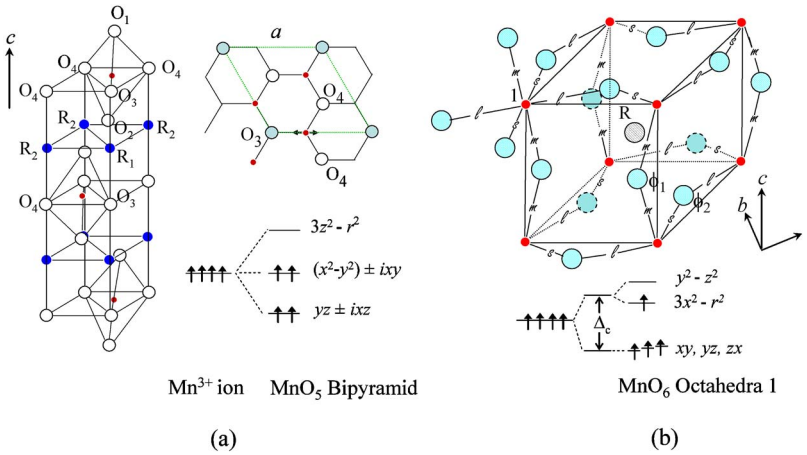

FIG. 1. (Color online) Schematic drawing of the crystal structure and the 3*d* orbitals in the MnO_n polyhedron for (a) hexagonal and (b) perovskite $R\mathrm{MnO_3}$. The dashed line in the middle picture shows the unit cell in the *ab* plane of the hexagonal phase.

as starting materials for high-pressure synthesis. A synthesis condition of 40 kbar and 1000 °C was sufficient to convert the hexagonal phase of all the Group II compounds into the perovskite phase. The high-pressure products were single phase from powder x-ray diffraction with a scan step of 0.02°/10 s. Structural parameters were obtained by fitting the x-ray diffraction patterns with the Rietveld method (FULLPROF). Whereas the refinements listed in Table I for the perovskite phase went as well as shown in Fig. 2, the reliability factors for refinements of the hexagonal phase were generally poor. Therefore, we list only the lattice parameters for the hexagonal phase in Table I. All good refinements of the hexagonal phase in the literature have been based on data of neutron and synchrotron powder diffraction. It is difficult for laboratory x-ray powder diffraction to give an accurate profile for all the diffraction regions that are needed to refine a noncentrosymmetric structure, such as the hexagonal structure of the $R\mathrm{MnO_3}$.[8] Since the lattice parameters obtained for the hexagonal phase are consistent with those in the literature, we use reported structural data in the discussion of our thermal-conductivity results. As checked by the thermoelectric power, both perovskite and hexagonal phases are essentially oxygen stoichiometric. Measurements of magnetization $M(T)$ were performed with a SQUID magnetometer (Quantum Design). Samples were orientated with Laue back diffraction for the hexagonal phase and cut into rectangular bars $0.5\times0.5\times2.5$ mm for the thermal conductivity measurements, which were described previously.[9]

III. RESULTS AND DISCUSSION

As calculated with the program SPUDS,[10] $R\mathrm{MnO_3}$ and $R\mathrm{FeO_3}$ have the identical Goldschmidt tolerance factor *t* for a given R^{3+} ion. Therefore, the structural transformation from the perovskite to the hexagonal phase occurring between Dy and Ho in $R\mathrm{MnO_3}$ prepared under ambient pressure is NOT

TABLE I. Structural parameters of the perovskite and hexagonal phase of Group II $R\mathrm{MnO_3}$ family.

	Y	Ho	Er	Tm	Yb	Lu
Perovskite						
a(Å)	5.25975(2)	5.26030(2)	5.24189(3)	5.22797(4)	5.21844(4)	5.19841(2)
b(Å)	5.83535(2)	5.84270(2)	5.82571(3)	5.78618(4)	5.80109(4)	5.78445(3)
c(Å)	7.35568(3)	7.35798(3)	7.33965(4)	7.32732(5)	7.30282(5)	7.29936(3)
m(Å)	1.9437(3)	1.9322(3)	1.9266(5)	1.9420(5)	1.9240(8)	1.9374(5)
l(Å)	2.243(2)	2.214(3)	2.188(4)	2.183(4)	2.292(7)	2.242(4)
s(Å)	1.892(1)	1.927(2)	1.955(2)	1.920(2)	1.868(4)	1.861(3)
⟨Mn-O⟩	2.02613	2.02437	2.0232	2.015	2.028	2.0135
$\mathrm{Mn\text{-}O_I\text{-}Mn}$	142.2(1)	144.36(1)	144.51(2)	141.22(2)	143.12(3)	140.75(2)
$\mathrm{Mn\text{-}O_{II}\text{-}Mn}$	143.46(7)	143.25(8)	142.03(1)	143.65(1)	139.2(2)	142.5(1)
⟨Mn-O-Mn⟩	143.04	143.62	142.85	142.84	140.51	141.96
R_p	0.057	0.05	0.044	0.039	0.08	0.064
R_{wp}	0.076	0.067	0.063	0.05	0.13	0.084
χ^2	2.24	1.48	2.32	1.9	10	3.93
Hexagonal						
a(Å)	6.14666(5)	6.13820(4)	6.11704(4)	6.081(3)	6.06625(4)	6.04011(3)
c(Å)	11.4411(1)	11.4118(1)	11.4556(1)	11.3748(6)	11.3973(1)	11.3648(6)
c/*a*	1.861	1.859	1.873	1.871	1.879	1.881

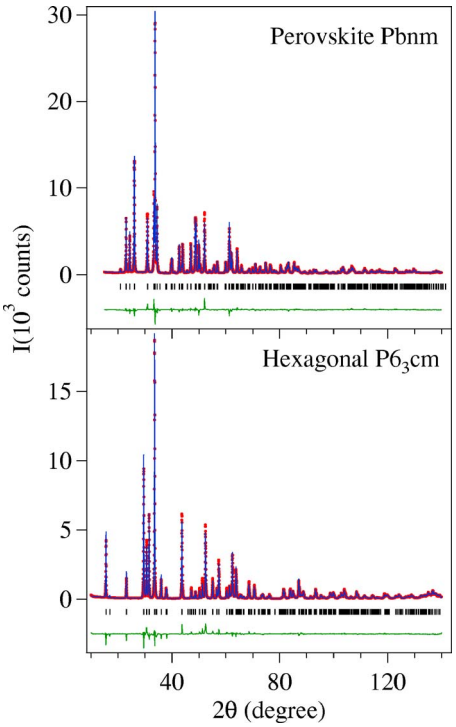

FIG. 2. (Color online) Powder x-ray diffraction and results of their profile fitting with the program FULLPROF for the perovskite and hexagonal $LuMnO_3$.

due to a t factor that is too small for the perovskite structure. Whether high pressure increases the t factor in this highly distorted perovskite structure remains to be determined by a structural study under high pressure. However, high pressure prefers the perovskite phase relative to the hexagonal phase because the phase transition increases the density: it increases in $YMnO_3$, for example, from 2.56 a.w./Å^3 for the hexagonal phase to 3.39 a.w./Å^3 for the perovskite phase. The density increase could also be used to account for the pressure-induced structural transformation from the garnet to the perovskite phase in $RGaO_3$.[1]

The $\chi(T)$ data of Fig. 3 for the hexagonal and perovskite phases of $YMnO_3$ and $LuMnO_3$ show Curie-Weiss behavior with the nearly identical Curie constant for each corresponding to a nearly spin-only μ_{eff} for the Mn^{3+} ions. However, a remarkably high $|\theta_w|/T_N \approx 10$ is found for the hexagonal phase where T_N is lowered by the frustrated magnetic coupling in the (001) planes; this ratio is close to unity in the perovskite phase where there is no geometric frustration of the spin-spin interactions. On the other hand, T_N in the hexagonal phase is about twice that of the perovskite phase, and the absolute value of the Weiss constant $|\theta_w|$ is enhanced by an order of magnitude in the hexagonal phase relative to its value in the perovskite phase. These data clearly show that the individual (180°-ϕ) Mn-O-Mn interactions in the (001) planes of the perovskite structure for the $RMnO_3$, where the bending angle ϕ in Table I is large, are lowered by a competition between the ferromagnetic e^1-O-e^0 component of the σ-bonding electrons and the antiferromagnetic t^3-O-t^3 component of the π-bonding electrons.

Figure 4 shows the $\kappa(T)$ and $1/\kappa(T)$ data for the hexagonal single crystals. The data for $HoMnO_3$ and $YMnO_3$ are

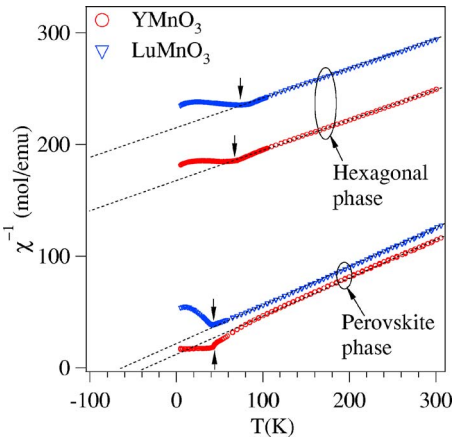

FIG. 3. (Color online) Temperature dependencies of inverse magnetic susceptibility of both the perovskite and hexagonal phases of $YMnO_3$ and $LuMnO_3$. All $RMnO_3$ members of Group II have been measured with a magnetic field of 5000 Oe. Only the results for $YMnO_3$ and $LuMnO_3$ for both phases are plotted here in order to show the magnetic response from the Mn-O array.

nearly identical to those reported by Sharma *et al.*[6] However, if we set aside the data for $YMnO_3$, our results for the hexagonal $RMnO_3$ family reveal a systematic change of $\kappa(T)$ with the R^{3+}-ion radius IR that is independent of the spin on the R^{3+} ion. This observation rules out any exchange-striction effect on $\kappa(T)$ associated with the spin fluctuations and therefore shows the suppression of $\kappa(T)$ below T_N in $HoMnO_3$ is a purely steric effect. In order to clarify the steric effect of the IR on $\kappa(T)$, we set aside the data for $YMnO_3$ since the Y^{3+} ion has a different chemistry than that of the rare-earth ions of similar size, a difference that can be noted in other RMO_3 perovskite families. Figure 4 shows that both $\kappa_{ab}(T)$ and $\kappa_c(T)$ are weakly temperature dependent in the

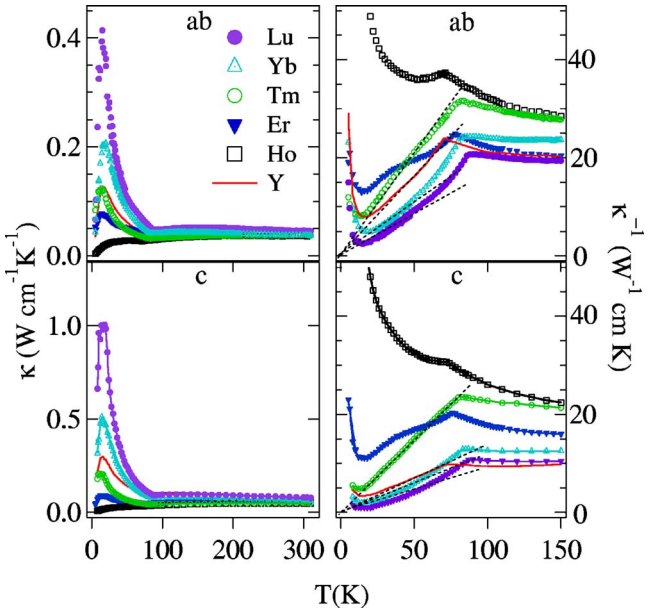

FIG. 4. (Color online) Temperature dependencies of thermal conductivity κ and κ^{-1} along the c axis and ab plane for single crystal samples of hexagonal $RMnO_3$.

TABLE II. Thermal conductivity at T_{ph} and 280 K for the hexagonal phase $R\mathrm{MnO_3}$.

	Y	Ho	Er	Tm	Yb	Lu
$\kappa_{ab}(T_{ph})$	12.6	2.78	7.7	12	20	39.3
$\kappa_c(T_{ph})$	30	3.1	8.95	20	51	100
$\kappa_c/\kappa_{ab}(T_{ph})$	2.38	1.11	1.16	1.6	2.5	2.56
κ_{ab}(280 K)	4.3	3.6	4.7	3.8	3.8	4.7
κ_c(280 K)	8.1	4.8	6.1	5	6.8	8.3
κ_c/κ_{ab}(280 K)	1.88	1.33	1.29	1.31	1.79	1.76

paramagnetic phase; they each undergo a broad maximum within the interval 150 K$<T<$200 K. A dramatic increase of $\kappa(T)$ below T_N for $\mathrm{LuMnO_3}$ decreases systematically with increasing *IR*. Although the absolute value of $\kappa(T)$ is always subject to the uncertainty of the sample's dimension and possible cracks within a crystal, the peak of $\kappa(T)$ below T_N decreases systematically in our crystals as the *IR* increases from Lu to Ho for both $\kappa_c(T)$ and $\kappa_{ab}(T)$. The temperature T_{ph} where $\kappa(T)$ peaks out is normally used as an indicator of a crystal's quality; the lower T_{ph}, the higher the quality.[11] A $T_{ph}\approx 15$ K indicates a superb quality of the crystals in this work. The $\kappa(T)$ on the side $T>T_{ph}$, as shown by $\kappa^{-1}(T)$ in Fig. 4, follows closely the $1/T$ law that is typical for a phonon thermal conductivity at temperatures above the Debye temperature.[11] $\mathrm{HoMnO_3}$ represents the extreme case where the $\kappa(T)$ at $T<T_N$ behaves essentially the same as the glassy $\kappa(T)$ at $T>T_N$. In the phase with magnetically ordered Mn^{3+}-ion spins, the evolution with decreasing *IR* from a glassy $\kappa(T)$ to a phonon-like $\kappa(T)$ in these high-quality crystals indicates that some lattice fluctuation not related to spin fluctuations on either the Mn^{3+} or the R^{3+} ions is suppressing the thermal conductivity. Moreover, a tiny change of $\kappa(T)$ on passing through T_N in $\mathrm{HoMnO_3}$ suggests that the same lattice fluctuation is primarily responsible for the glassy $\kappa(T)$ in the paramagnetic phase; and since spin ordering on the Mn array induces a structural transition that increases with decreasing *IR*, we are led to investigate what lattice fluctuation might be reduced by this distortion. The steric effect of the *IR* on $\kappa(T)$ is also visible in the paramagnetic phase, but it is much weaker than that in the magnetically ordered phase. In addition, the $\kappa(T)$ of the hexagonal $R\mathrm{MnO_3}$ phase is anisotropic as measured by the ratio of κ_c/κ_{ab}. It is also interesting to notice that this ratio is *IR* dependent. As shown in Table II, the heat conduction of hexagonal $R\mathrm{MnO_3}$ becomes increasingly anisotropic as the *IR* decreases in the magnetically ordered phase, whereas it becomes less anisotropic in the paramagnetic phase. The anisotropic $\kappa(T)$ has its roots in the structural features of the hexagonal phase, and questions how the anisotropic $\kappa(T)$ develops as a function of *IR* and why the *IR* dependence of the κ_c/κ_{ab} ratio shows a dramatic change from the paramagnetic phase to the magnetically ordered phase must be addressed with help from structural studies.

A very important feature of the hexagonal structure with space group $P6_3cm$ is the oxygen triangle consisting of two oxygen positions O_3 and O_4 and a Mn located at the center as illustrated in Fig. 1(a). The symmetry of the space group allows the Mn to move along the *x* direction, which shortens two Mn-O_4 bond lengths and enlarges the Mn-O_3 bond length. The temperature dependence of this local structural change may provide an important clue to interpret the anomalous $\kappa(T)$ of hexagonal $R\mathrm{MnO_3}$. For this purpose, we turn our attention to recent structural data for $\mathrm{YMnO_3}$ since the most complete and accurate neutron powder diffraction data set has been made available for this compound.[7] On lowering the temperature, the Mn-O_3 and Mn-O_4 bond lengths show the most dramatic change among all the Mn-O and Y-O bond lengths in the hexagonal structure. Moreover, a larger c/a ratio reflects a larger cooperative rotation of the MnO_5 sites. Therefore, the temperature dependence of the lattice c/a ratio and the Mn-O_3 and Mn-O_4 bond lengths from the study have been plotted along with $\kappa(T)$ data in Fig. 5. Although we have set aside the $\kappa(T)$ data for $\mathrm{YMnO_3}$ from the results for the other $R\mathrm{MnO_3}$ compounds in order to clarify the steric effect of thermal conductivity, we use the structural data set for $\mathrm{YMnO_3}$ to investigate the lattice fluctuations that suppress $\kappa(T)$ for the other $R\mathrm{MnO_3}$ compounds because that is what is available. Since Y^{3+} has a slightly different chemistry than the rare earths, the evolution of $\kappa(T)$ vs *IR* does not reflect the true steric effect. However, $\mathrm{YMnO_3}$ shares a similar temperature dependence of crystal structure with the other hexagonal $R\mathrm{MnO_3}$ compounds as is proven by comparing $\mathrm{YMnO_3}$ with $\mathrm{LuMnO_3}$. Unfortunately, the study[8]

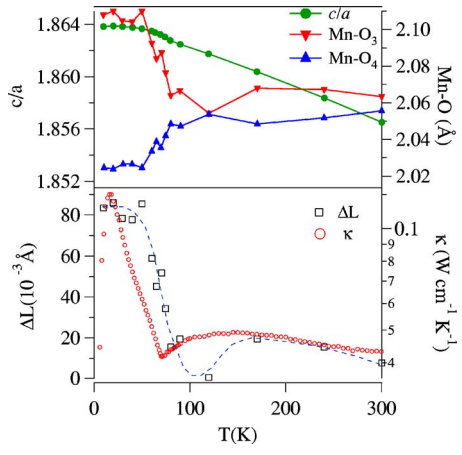

FIG. 5. (Color online) Temperature dependencies of the c/a ratio, Mn-O bond lengths and the thermal conductivity κ within the *ab* plane of hexagonal $\mathrm{YMnO_3}$. $\Delta L=$(Mn-O_3)−(Mn-O_4) is proportional to the distance of the Mn from center of the MnO_3 triangle. The structural data are from Ref. 7.

of $LuMnO_3$ was made within a relatively narrow temperature range.

Figure 5 shows that the Mn-O_3 and Mn-O_4 bond lengths are nearly identical at room temperature. As temperature decreases, the two bond lengths split a little and become identical again before separating completely below T_N. This change indicates that the Mn is loosely bound within the oxygen triangle. As illustrated in Fig. 1(a), the Mn moves away from O_3 along the x direction within the MnO_3 triangle below T_N; this motion represents a soft-mode phase transition where the Mn is permanently displaced from the center of the triangle. It is clear that the Mn ion remains rattling along the x direction at $T>T_N$; at $T<T_N$, the soft-mode displacement restores the phonon contribution to $\kappa(T)$ in $YMnO_3$. The bond length difference ΔL between Mn-O_3 and Mn-O_4, which reflects the change of the average Mn position along the x direction relative to the center of the triangle, varies with temperature. More interestingly, the temperature dependence of ΔL resembles the essential feature of $\kappa(T)$. Therefore, we conclude that Mn rattling along the Mn-O_3 bonding direction suppresses the thermal conductivity in the hexagonal $RMnO_3$ phase. The progressive change from a glassy $\kappa(T)$ in $HoMnO_3$ to the phonon-like $\kappa(T)$ in $LuMnO_3$ below T_N suggests that the Mn ions remain rattling in hexagonal $HoMnO_3$, whereas they behave as regular lattice vibrations in $LuMnO_3$. We monitor this evolution by studying the anisotropic $\kappa(T)$ in the hexagonal structure.

The slightly anisotropic $\kappa(T)$ in the paramagnetic phase that is found in all members of the hexagonal $RMnO_3$ family is due to the anisotropic crystal structure. In the magnetically ordered phase below T_N, however, the striking evolution from the glassy $\kappa(T)$ in $HoMnO_3$ to the phonon-like $\kappa(T)$ in $LuMnO_3$ is associated with an obvious increase of the ratio κ_c/κ_{ab}. In other words, the $RMnO_3$ crystal becomes highly anisotropic to thermal conduction if the phonon thermal conductivity is restored. The crossover from a glassy $\kappa(T)$ to the phonon-like $\kappa(T)$ can be induced either by reducing the IR in the magnetically ordered phase or by lowering the temperature through T_N in the hexagonal $RMnO_3$ family (R = Y, Tm, Yb, Lu). We take $YMnO_3$ as an example to demonstrate the correlation between the structural distortion and the development of an anisotropic $\kappa(T)$ on lowering the temperature. As shown in Fig. 5 and Table II, the development of the anisotropy of $\kappa(T)$ corresponds to an increasing c/a ratio of the lattice parameters. By studying the crystal structure of $YMnO_3$ at high temperature, Van Aken and Palstra[8] have shown that the ferrielectric phase is characterized by a rotation of the MnO_5 polyhedra around the axis parallel to O_4-O_4; the rotation also displaces the Y^{3+} ions. This rotation also displaces the O_3 atoms twice as far as the O_4 atoms out of the (001) plane, which requires the (Mn-O_4) bond length to be shortened if the Mn is to remain in the basal plane. Thus the bipyramidal rotations lower the potential at a position removed from the centroid of the site that competes with the potential at the centroid. This competition becomes stronger the greater the rotation of the bipryamidal sites, so the Mn vibrations parallel to the x axis become softer as the rotation increases. On lowering the temperature through T_N, exchange striction enhances the rotation of the bipyramidal sites, but a rigid rotation is hindered by the contact of the O_1 and O_2 atoms with the R^{3+} ions. A smaller IR allows a greater rotation; and the greater rotation in the presence of the smaller R^{3+} ions allows the Mn to be displaced to a new equilibrium position having a shorter (Mn-O_4) than (Mn-O_3) bond length. Since the Mn-site rotations displace the R^{3+} ion along the c axis, they also increase the lattice c/a ratio. Figure 5 shows that the c/a ratio of $YMnO_3$ increases on lowering the temperature, which signals a softening of the Mn vibrations; a small jump in the c/a ratio on cooling through T_N marks the rotation at which the Mn atoms become displaced to a new equilibrium position. Once the new equilibrium position is established, the phonon thermal conductivity is restored. The Ho^{3+} ion of $HoMnO_3$ has the largest IR of all the hexagonal $RMnO_3$ family and therefore presents the largest resistance to the Mn-site rotations. Consequently, $HoMnO_3$ has the smallest c/a ratio as shown in Table I, and the site rotations are never large enough to stabilize the off-centroid potential sufficiently to induce a static displacement of the Mn to a new equilibrium position. Therefore, a glassy $\kappa(T)$ remains to lowest temperatures in the hexagonal $HoMnO_3$ crystal. We therefore conclude that softening of the x-axis Mn vibrations along the Mn-O_3 bonding direction is the dominant factor suppressing the phonons in the hexagonal $RMnO_3$ family. Exchange striction associated with short-range magnetic order above T_N may enhance this effect in the temperature interval $T_N<T<150$ K, but it is not the dominant player.

The rattling motion of heavy atoms within the cage structure formed by relatively lighter atoms has been identified to be a key factor for suppressing the thermal conductivity in skutterudites[12] and clathrates.[13] In all cases, the heavy atoms are loosely bound in the cages, which gives rise to the low frequency (<100 cm^{-1}) rattling vibrational modes as seen in Raman spectrum. These vibrations can scatter the acoustic phonons from the framework atoms, thus reducing the lattice thermal conductivity. The rattling motion has also been found in silicate garnets where the low frequency mode is assigned to the rattling motion of the light atom Mg in the plane of the longer Mg-O_4 bonds in pyrope.[14] Unfortunately, the Raman data of the hexagonal $RMnO_3$ available to us have been collected at $f>100$ cm^{-1} Raman shift.[15,16] Raman optical study on low-frequency modes in the hexagonal $RMnO_3$ is invited in order to confirm the rattling motion of Mn ion if they are Raman active.

In contrast to the hexagonal phase, the Mn^{3+} ion in the $MnO_{6/2}$ octahedra of the perovskite phase is JT active. The cooperative JT distortion orders the e orbital in the 001 plane and modifies the $MnO_{6/2}$ octahedra to have long, medium, and short Mn-O bond lengths as shown in Fig. 1(b) and Table I. There is no space for a Mn^{3+} ion to rattle in this perovskite structure. Therefore, although $\kappa(T)$ is reduced by grain-boundary scattering in our ceramic samples of the perovskite phase, the phonon-like thermal conductivity within 100–300 K is easily recognized in Fig. 6. In the perovskites $YMnO_3$ and $LuMnO_3$, $\kappa(T)$ peaks out around a $T_{ph}\approx 100$ K, which is typical for ceramic samples showing phonon-like thermal conductivity. The magnitude of T_{ph} is related inversely to the longest mean free path for phonon

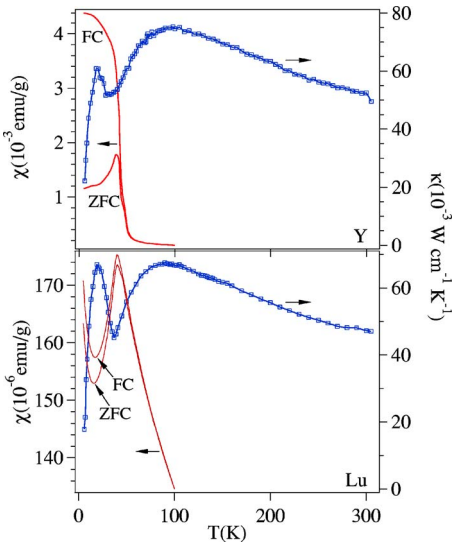

FIG. 6. (Color online) Temperature dependencies of magnetic susceptibility χ and thermal conductivity κ for the perovskite phase of Group II $R\mathrm{MnO_3}$ familay. $\chi(T)$ was measured under 20 Oe in order to track down T_N precisely. The $\chi(T)$ shown for $\mathrm{LuMnO_3}$ was measured under 500 Oe since the data under 20 Oe are a little noisy, but they are identical. Results of $\kappa(T)$ for other perovskite $R\mathrm{MnO_3}$ are not shown because those samples are too porous to give reliable data.

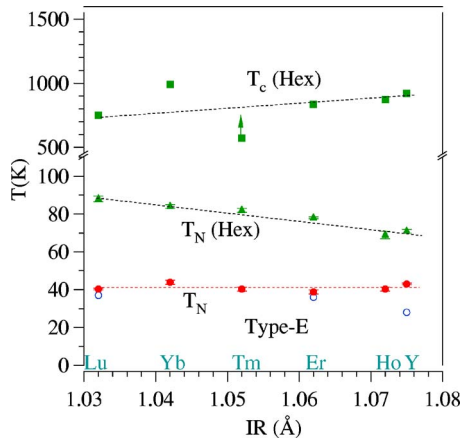

FIG. 7. (Color online) The phase diagram of transition temperatures for both hexagonal and perovskite phases vs *IR*. The T_N is obtained from both $\chi(T)$ and $\kappa(T)$ data. T_N obtained from $\chi(T)$ and $\kappa(T)$ are nearly identical for the hexagonal $R\mathrm{MnO_3}$, but T_N from $\kappa(T)$ shown by open circle symbols are slightly lower than those from $\chi(T)$ for the perovskite $R\mathrm{MnO_3}$. The ferroelectric Curie temperature T_c is from Ref. 20.

transport, which is limited to the grain size or the density of impurities. Therefore, a huge difference between $T_{\mathrm{ph}} \approx 15$ K in the hexagonal phase and the $T_{\mathrm{ph}} \approx 100$ K in the perovskite phase reflects a significant difference of the phonon mean free paths between the single crystal and ceramic samples. On further lowering the temperature, a sharp minimum of $\kappa(T)$ occurs near the spin-ordering temperature T_N; it resembles the critical-scattering effect on $\kappa(T)$ found in other magnetic insulators.[17,18] However, the minimum of $\kappa(T)$ occurs at a temperature that is a few Kelvin lower than T_N as measured by the magnetic susceptibility. It is important to note the evolution of $\kappa(T)$ in the vicinity of T_N as a function of the structural distortion in the perovskite phase; it shows only a slope change at T_N in the perovskite $\mathrm{LaMnO_3}$,[9] whereas it develops a sharp minimum in the perovskite phase of $\mathrm{YMnO_3}$ and $\mathrm{LuMnO_3}$. The structural data listed in Table I suggest that the perovskite $R\mathrm{MnO_3}$ phase synthesized under high pressure has the same orbital ordering as in $\mathrm{LaMnO_3}$. However, the average Mn-O-Mn bond angle is reduced from 155° in $\mathrm{LaMnO_3}$ to 142° in $\mathrm{LuMnO_3}$, as shown in Table I, which reduces the ferromagnetic coupling via the σ bond e^1-O-e^0 interactions much more than the antiferromagnetic coupling via the π bond t^3-O-t^3 interactions in the same Mn-O-Mn bonds of the (001) plane. Competition between these two components may be the origin for the transition from type-A to type-E antiferromagnetic ordering[19] without change in the orbital ordering. In contrast to the Type-A spin-ordering phase in the $R\mathrm{MnO_3}$ perovskites with light rare-earth ions where T_N is extremely sensitive to *IR*, T_N in the type-E spin-ordered phase is essentially independent of *IR*, see Fig. 7. This observation supports the exchange-competition mechanism proposed for the type-E phase. Moreover, this deduction is also supported by Fig. 6 since magnetic-coupling fluctuations above T_N between ferromagnetic and antiferromagnetic interactions in the (001) planes of the pressure-stabilized $R\mathrm{MnO_3}$ perovskite phase would significantly enhance the spin critical scattering, which normally causes only a weak modification of $\kappa(T)$ near T_N in a magnetic insulator.

IV. CONCLUSIONS

In conclusion, a systematic study of the thermal conductivity $\kappa(T)$ for the entire hexagonal $R\mathrm{MnO_3}$ family and comparison with the structural evolution with temperature of the $\mathrm{MnO_5}$ bipyramidal sites in $\mathrm{YMnO_3}$ have revealed that the dominant factor suppressing $\kappa(T)$ is a softening of the Mn vibrations in the Mn-$\mathrm{O_3}$ bonding direction as the Mn potential of an off-centroid position is progressively stabilized by an increasing rotation of the Mn sites. These site rotations are responsible for the ferrielectricity of these samples and their magnitude increases with decreasing size of the R^{3+} ions they displace from the RO planes. For the smaller rare-earth ions, exchange striction increases these rotations sufficiently below T_N to induce a soft-mode transition to a new structure in which the Mn atoms are displaced from the $\mathrm{O_3}$ toward the two $\mathrm{O_4}$ atoms of the triangular oxygen plane of the bipyramidal sites. Phonons are restored in this new phase. However, the largest $\mathrm{Ho^{3+}}$ ion of the hexagonal $R\mathrm{MnO_3}$ family restrains the bipyramidal-site rotations, and rotations remain too small below T_N to stabilize the new structure. Therefore, the Mn-atom vibrations along Mn-$\mathrm{O_3}$ bonding direction continue to suppress $\kappa(T)$ below T_N in the hexagonal $R\mathrm{MnO_3}$ phase with a larger R=Ho or Er; and exchange striction associated with short-range order of the Mn spins may induce site-rotation fluctuations above T_N that enhance the softening of the Mn vibration, but exchange

striction is not the dominant factor causing the suppression of $\kappa(T)$. The perovskite phase of these same $R\mathrm{MnO}_3$ compounds shows a phonon-like $\kappa(T)$ at high temperatures and a sharp minimum of $\kappa(T)$ near T_N due to an anomalously large critical spin scattering. The type-E spin ordering found below T_N in these compounds is characterized by an enhanced critical scattering and a Néel temperature T_N that is independent of the R^{3+}-ion radius. These observations and a comparison of the paramagnetic susceptibilities of the two phases for the same compound provide support for the suggestion[19] that the type-E magnetic order is a consequence of a crossover from a net ferromagnetic to a net antiferromagnetic Mn-O-Mn interaction in the (001) planes of the orthorhombic perovskites.

ACKNOWLEDGMENTS

We thank the NSF Grant Nos. DMR 0555663 and DMR 0353362 (U.S.-European collaboration) and the Robert A. Welch Foundation, Houston, Texas, for financial support.

[1] M. Marezio, J. P. Remeika, and P. D. Dernier, Inorg. Chem. **7**, 1337 (1968).
[2] A. Waintal and J. Chenavas, Mater. Res. Bull. **2**, 819 (1967).
[3] J. A. Alonso, M. J. Martinez-Lope, M. T. Casais, and M. T. Fernandez-Diaz, Inorg. Chem. **39**, 917 (2000).
[4] Bas B. Van Aken, T. T. M. Palstra, A. Filippetti, and N. A. Spaldin, Nat. Mater. **3**, 164 (2004).
[5] T. Katsufuji, M. Masaki, A. Machida, M. Moritomo, K. Kato, E. Nishibori, M. Takata, M. Sakata, K. Ohoyama, K. Kitazawa, and H. Takagi, Phys. Rev. B **66**, 134434 (2002).
[6] P. A. Sharma, J. S. Ahn, N. Hur, S. Park, S. B. Kim, S. Lee, J.-G. Park, S. Guha, and S-W. Cheong, Phys. Rev. Lett. **93**, 177202 (2004).
[7] S. Lee, A. Pirogov, J. H. Han, J.-G. Park, A. Hoshikawa, and T. Kamiyama, Phys. Rev. B **71**, 180413(R) (2005).
[8] Bas B. Van Aken and T. T. M. Palstra, Phys. Rev. B **69**, 134113 (2004).
[9] J.-S. Zhou and J. B. Goodenough, Phys. Rev. B **66**, 052401 (2002).
[10] M. W. Lufaso and P. M. Woodward, Acta Crystallogr., Sect. B: Struct. Sci. **B57**, 725 (2001).
[11] R. Berman, *Thermal Conduction in Solids* (Clarendon, Oxford, 1976).
[12] B. C. Sales, D. Mandrus, B. C. Chakoumakos, V. Keppens, and J. R. Thompson, Phys. Rev. B **56**, 15081 (1997).
[13] D. Nataraj and J. Nagao, J. Solid State Chem. **177**, 1905 (2004).
[14] B. A. Kolesov and C. A. Geiger, Phys. Chem. Miner. **27**, 645 (2000).
[15] M. N. Iliev, H.-G. Lee, V. N. Popov, M. V. Abrashev, A. Hamed, R. L. Meng, and C. W. Chu, Phys. Rev. B **56**, 2488 (1997).
[16] A. P. Litvinchuk, M. N. Iliev, V. N. Popov, and M. M. Gospodinov, J. Phys.: Condens. Matter **16**, 809 (2004).
[17] H. Stern, J. Phys. Chem. Solids **26**, 153 (1965).
[18] F. B. Lewis and N. H. Saunders, J. Phys. C **6**, 2525 (1973).
[19] J.-S. Zhou and J. B. Goodenough, Phys. Rev. Lett. **96**, 247202 (2006).
[20] Th. Lonkai, D. G. Tomuta, U. Amann, J. Ihringer, R. W. Hendrikx, D. M. Tobbens, and J. A. Mydosh, Phys. Rev. B **69**, 134108 (2004).